HiSST: 2nd International Conference on
High-Speed Vehicle Science & Technology

11–15 September 2022, Bruges, Belgium

On the design of a Mach 5 axisymmetric contoured nozzle for the VKI H3 hypersonic tunnel

Bora O. Cakir [1], *Guillaume Grossir* [2], *Sébastien Paris* [3], *Bayindir H. Saracoglu* [4]

Abstract

The operational map of the H3 Mach 6 blowdown wind tunnel, operated at the von Karman Institute for Fluid Dynamics (VKI), is extended towards lower Mach numbers. The main characteristics of the present wind tunnel facility are first reviewed and their performance restrictions are analyzed. Accordingly, the operating regimes and the corresponding performance characteristics of the supersonic ejector is investigated as it is identified to be the most critical component for achieving the desired modifications. Then, the design methodology of a new contoured axisymmetric nozzle enabling operation at Mach 5 and high Reynolds numbers is reported. The design space for the new nozzle is analyzed by means of a parametric study for the nozzle contour and an optimum set of parameters that yields the best performances are identified (core flow diameter, Reynolds number). The design space is confined in order to meet the different design constraints associated with the existing framework (i.e. dimensional restrictions, ejectable mass flow rates, heating requirements). Finally, Navier-Stokes computations of the flow development over the newly designed Mach 5 nozzle are performed to serve as an estimate of the expected radial and axial flow uniformity within the core flow.

Keywords: *VKI H3 wind tunnel, hypersonic, contoured nozzle design, HYPNOZE, method of characteristics, viscous correction, supersonic ejector, blow-down facility*

Nomenclature

Latin

d^* – nozzle throat diameter, m
M – Mach number
p – pressure, Pa
r^* – nozzle throat radius, m
R – ratio of throat radius of curvature to throat radius
R_c – throat radius of curvature, m
T – temperature, K
u – axial flow velocity, m/s
x, y – Cartesian coordinates, m
X_{BC} – dimensionless distance between points B and C, $X_{BC} = \frac{x_C - x_B}{r_{cr}}$

Greek

δ – boundary layer thickness, m
δ^* – boundary layer displacement thickness, m
θ – flow angle, degrees
ρ – density, kg/m^3
ω – nozzle opening angle, degrees

Superscripts

’ – Primary stream
” – Secondary stream

Subscripts

0 – Stagnation flow conditions

[1] *Doctoral Candidate, VKI (von Karman Institute for Fluid Dynamics), Turbomachinery and Propulsion Department, Chaussée de Waterloo 72, Rhode-Saint-Genèse, cakir@vki.ac.be*
[2] *Senior Research Engineer, VKI (von Karman Institute for Fluid Dynamics), Aeronautics and Aerospace Department, Chaussée de Waterloo 72, Rhode-Saint-Genèse*
[3] *Senior Research Engineer, VKI (von Karman Institute for Fluid Dynamics), Aeronautics and Aerospace Department, Chaussée de Waterloo 72, Rhode-Saint-Genèse*
[4] *Research Expert, VKI (von Karman Institute for Fluid Dynamics), Turbomachinery and Propulsion Department, Chaussée de Waterloo 72, Rhode-Saint-Genèse*

1. Introduction

The development of sustainable high-speed travel systems requires a significant amount of joint numerical and experimental investigations. In order to evaluate the aerodynamic performances of these vehicles and validate numerical analysis performed by means of computational fluid dynamics (CFD) tools, extended operational maps of existing ground testing facilities may be required. The VKI-H3 hypersonic wind tunnel has been utilized for multiple experimental studies investigating various aspects of flight performance characteristics of high-speed aerial vehicles. Accordingly, hypersonic flow characterizations around blunted cone–flare are performed and the obtained results are employed for experimental validation purposes [1, 2]. Multiple studies of hypersonic boundary layer transitions due to interactions with roughness elements are conducted [3–5]. Moreover, experimental characterization of the design specifications of the Expert (European eXPErimental Re-entry Testbed) PL4/PL5 vehicle is performed with a specific concentration of various modes of transition triggering [6]. Furthermore, the boundary layer instabilities on the same space vehicle during atmospheric reentry are investigated by means of capturing surface pressure fluctuations [7]. Moreover, aerothermal effects of ablation and heat-shield components on the aerodynamic performance of re-entry capsules are captured [8]. Finally, experimental characterization of liquid jet atomization [9] and flow topology around gas, liquid, and three-dimensional obstacles exposed to hypersonic cross-flow [10] are studied.

All of the aforementioned experimental campaigns are conducted for models that contain M_∞ ~6 in their operational envelope. However, within the context of EU H2020 More & Less project, the high-supersonic case study is conducted at a design flight Mach number for the cruise stage of $M_\infty = 5$. Thus, in order the conduct the necessary ground testing of the cruise conditions, modifications are foreseen to the VKI-H3 hypersonic tunnel in order to widen its operational capabilities for which a freestream Mach number of M_∞=5 and large Reynolds numbers are targeted. In this regard, the facility layout of the VKI H3 wind tunnel is analyzed to identify the critical components bounding the operational space of the wind tunnel. Accordingly, the parameters constraining the design space for the new Mach 5 nozzle are investigated over a parametric study to yield the range of design specifications for the new nozzle. Then, details of the nozzle design and optimization procedure are described resulting in the final viscous corrected geometric form of the new Mach 5 nozzle form.

1.1. The VKI H3 wind tunnel and the existing framework

The VKI-H3 wind tunnel (Fig. 1) is a low enthalpy, blow-down facility designed to generate hypersonic flows at large Reynolds numbers [11]. It is currently equipped with an axisymmetric contoured nozzle producing a uniform Mach 6 free jet with an inviscid diameter of 120 mm [12, 13]. Dried air is supplied from a pebble-bed heater at stagnation pressures from 7 to 35bar at a maximum stagnation temperature of 550K. The free-stream unit Reynolds number may be varied from 3x10^6 to 30x10^6/m with the current Mach 6 nozzle. Once the desired the stagnation pressure and temperature conditions are established, a fast activating valve is opened and the air is expanded through a contoured nozzle into a vacuumed test chamber. A supersonic diffuser (located immediately downstream of the test chamber) is used to decelerate the flow and recover the kinetic energy in the form of pressure. A supersonic ejector is then used to discharge the nozzle mass flow rate into the atmosphere.

The test section is equipped with a high-accuracy five-degree-of freedom orientation and a rapid injection mechanisms where the letter enables model injection into the hypersonic stream in less than 0.1s. Typical useful test times extend up to 30s. Advanced instrumentation is available for both localized (thermocouples, pressure sensors) and global measurement techniques (Infra-Red, 3-components balances) by means of a National Instruments data acquisition system. Additional measurement techniques may be used for specific needs. The tunnel is also equipped with high-quality shadowgraph and schlieren optical systems.

1.2. Mach 6 axisymmetric contoured nozzle of the VKI H3 wind tunnel

The existing Mach 6 axisymmetric contoured nozzle is characterized by a length of 760 mm and an exit diameter of 155 mm. It is operated with dry air right above the flow condensation threshold so that it yields the largest free-stream unit Reynolds numbers (typically reaching up to Re_{unit}=30x10^6/m). This Mach 6 nozzle dates back to the 60s and was initially designed with an interchangeable throat in such a way that slightly different Mach numbers could eventually be achieved within the test section at the

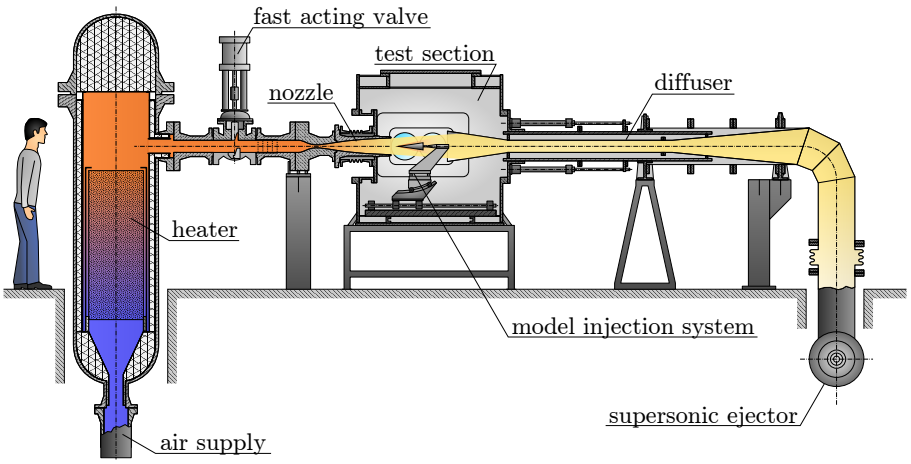

Fig 1. Schematic representation of H3 hypersonic wind tunnel facility.

expense of slightly degraded flow uniformity [14, 15]. It seems this was never realized in practice and this nozzle was kept operated at its targeted design conditions.

2. Facility sizing and operation

Nowadays, as the need to operate the facility at lower Mach numbers becomes increasingly important, new nozzles are required. Rather than fitting the existing nozzle with a new throat that would compromise the flow uniformity at the test section, a new nozzle is designed and optimized in order to fit within the existing hardware. The objective of this work is to extend the operational capabilities of the H3 tunnel towards lower Mach numbers. Besides the required design of a new contoured nozzle, it also implies to account for all the constraints associated with the existing framework. In particular, reducing the testing Mach number from 6 to 5 is associated with a decrease of the nozzle exit to throat area ratio. Hence, sticking to the throat diameter used for the Mach 6 nozzle would lead to an unacceptable reduction ($\sim$48%) of the test cross-sectional area. Thus, in order to achieve sufficiently large core flow dimensions which can then be useful for testing purposes, the throat size needs to be increased which requires the facility to accommodate a larger mass flow.

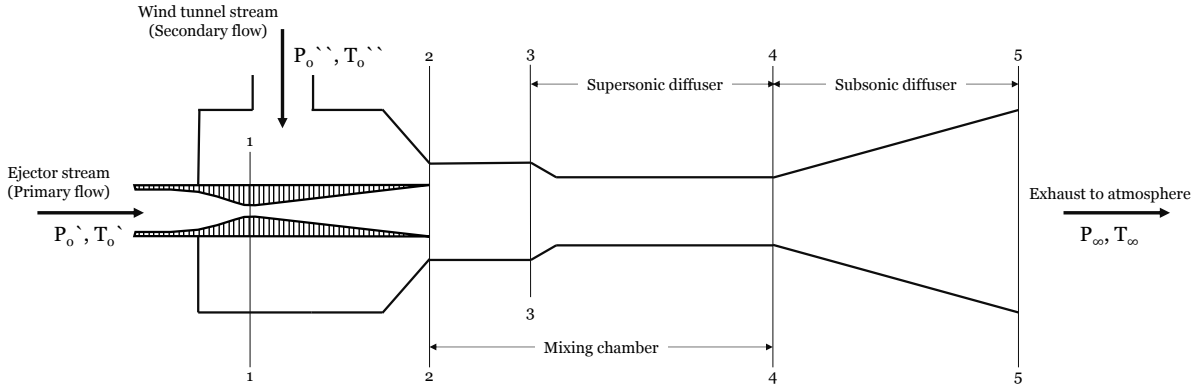

Fig 2. Schematic representation of supersonic ejector in operation at the H3 hypersonic wind tunnel facility.

2.1. Supersonic ejector

The purpose of a supersonic ejector is to draw a given mass of secondary flow (wind tunnel stream) from a reservoir of low pressure into a region of higher pressure by means of two main driving forces. One of these forces being the pressure gradients due to the vacuum created by the accelerated ejector

(primary) stream from a given reservoir and second one being the shear forces between the low speed secondary stream and the high-speed primary stream [16]. The reservoir of secondary flow refers to the recovered wind tunnel stream downstream of the test chamber and supersonic diffuser. The ejector stream is drawn from the primary reservoir with a given stagnation pressure and provided into the mixing chamber by means of a supersonic nozzle that accelerates the flow and creates the desired vacuum conditions. The primary and secondary stream come into contact tangentially in the mixing chamber before being discharged to the atmosphere [17].

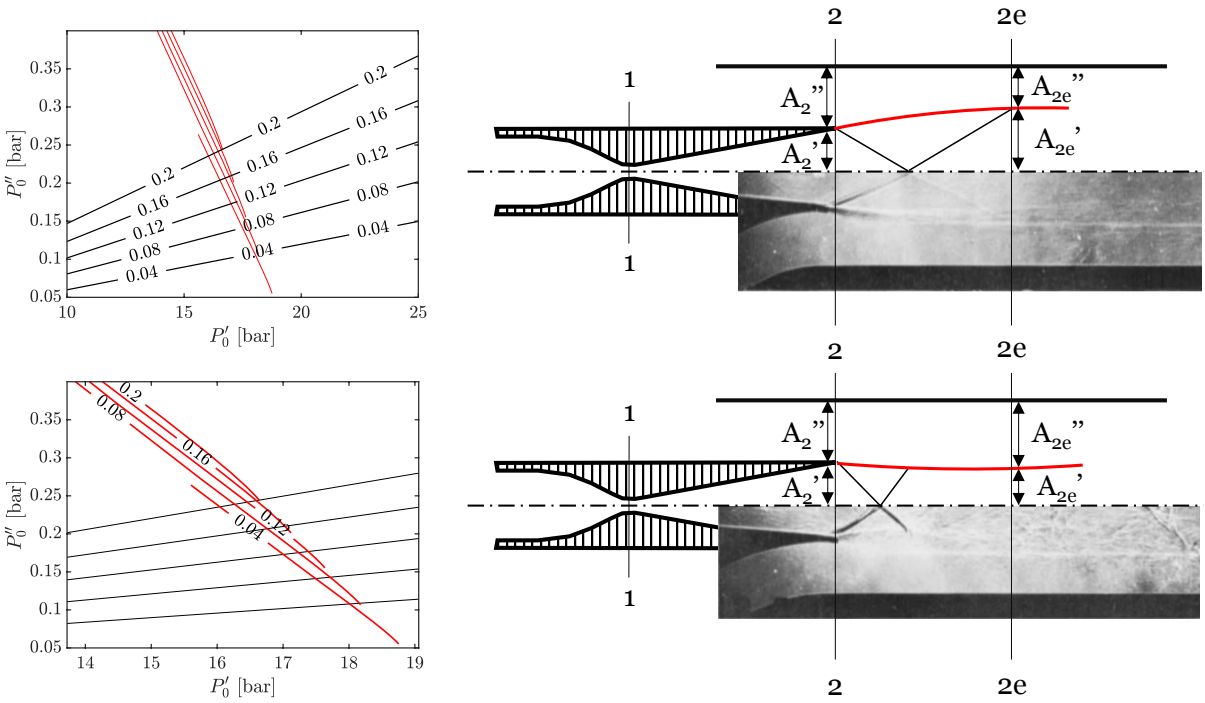

Fig 3. Mass rate of ratios of secondary to primary stream (μ) with varying stagnation pressures for supersonic (top-left) and mixed (bottom-left) flow regimes. Schematics and experimental shadowgraph images [16] of flow development within the mixing chamber for supersonic (top-right) and mixed (bottom-right) flow regimes.

Supersonic ejector operation is determined by the reservoir pressures relative to each other and the atmospheric conditions [18]. For high values of ejector reservoir pressure, the primary flow exits the ejector nozzle at supersonic conditions and remains supersonic throughout the mixing chamber. Due to the persistent supersonic conditions, the information transfer direction is consistently downstream. Hence, the downstream pressure dictated by the exhaust conditions does not constraint or influence the ejector operation. Moreover, depending on the speed of secondary stream entering the mixing chamber, saturated supersonic conditions might be obtained if the secondary stream becomes chocked at the section of interaction with the primary stream due to the increasing stagnation pressure of secondary flow [19]. Furthermore, as the primary reservoir pressure is decreased, the supersonic jet extending through the mixing chamber breaks and the corresponding shock train moves towards the ejector nozzle. Due to the proceeding subsonic primary flow and the subsonic secondary flow, the exhaust pressure conditions become effective determining the mixing behavior of the primary and secondary streams limiting the amount of mass flow that can be drawn from the secondary reservoir [20].

2.1.1. Operating regimes

The flow properties within the ejector can be described by means of one dimensional inviscid flow equation in order to explore the complete operational space of the supersonic ejector in a reduced order

manner. Thus, referring to the aforementioned regimes of supersonic and mixed flow patterns, the governing equation set relating to the corresponding flow development throughout the ejector can be derived using momentum and mass conservation relations. In this regard, in case of the supersonic flow pattern two main assumptions can be made. Firstly, both wind tunnel (secondary) and ejector (primary) stream are assumed to be expanded isentropically between sections 2 and 2e. Hence, stagnation flow properties are preserved. As shown in Fig. 3, high reservoir pressure of primary stream allows the streamtube exiting the ejector nozzle to expand towards the secondary stream over the shear layers. Accordingly, the shear layer acts as an effective compression surface for the secondary stream and accelerates the flow by imposing a contraction of the local flow cross-section since $M_{S,1}$ <1. Secondly, it is assumed that the formation of the shear layers is such that the secondary stream reaches sonic conditions at section 2e which acts as a sonic throat. Thus, the ratio of mass flow rates is computed by means of recasting the momentum balance between sections 2 and 2e (Eq. 1).

$$\mu = \frac{\dot{m}''}{\dot{m}'} = \sqrt{\frac{T_0'}{T_0''}} \frac{f_1(M_{2e}') - f_1(M_2')}{f_1(M_2'') - f_1(M_{2e}'')} \tag{1}$$

f_1 is a user defined function of local Mach number of the corresponding stream, $f_1 = f_1(M)$ (Eq.2). Accordingly, the Mach number of the ejector stream at the exit of the ejector nozzle is known from the geometric properties of the ejector, A_2'/A_1'. Moreover, the flow of primary stream reaches sonic condition at section 2e for the supersonic flow pattern , $M_{2e}'' = 1$ (Fig. 3). Thus, the area ratio of the primary and secondary streams (A_2e''/A_2'') can be computed for a range of Mach numbers of the secondary stream at section 2 (M_2'').

$$f_1(M) = \frac{M+1}{\gamma M \sqrt{1 + \frac{1}{2}(\lambda - 1)M^2}} \tag{2}$$

Furthermore, as the flow speed of the secondary stream is sufficiently high, the secondary stream reaches the sonic condition at section 2 upstream of 2e where the flow conditions of primary and secondary streams are defined at the respective choking positions, $M_{S,2}$=1 and $M_{P,1}$=1. Hence, the ratio of mass flow rates (μ) is described by the corresponding geometric properties of the ejector system and the reservoir pressures of primary and secondary streams using Eq. 3.

$$\mu = \frac{\dot{m}''}{\dot{m}'} = \frac{A_2''}{A_1'} \frac{P_0''}{P_0'} \tag{3}$$

Moreover, reducing the reservoir pressure of the ejector stream, reduces the length of the fully supersonic portion of the flow field within the mixing chamber prior to reaching the second throat. Then, although the primary flow at section 2 is supersonic, the supersonic flow is not maintained throughout the mixing chamber which means that the flow regions near the mixing chamber walls are subsonic. This regime of coexisting supersonic and subsonic flow condition throughout the cross-section of the mixing chamber is referred to as the mixed flow pattern. Due to the supersonic flow being confined to the core flow occupied by the primary stream, the secondary stream is an exposed to being affected by the exhaust pressure, P_4. Thus, the momentum transfer between sections 2 and 4 is expressed by Eq. 4.

$$P_0' A_2' f_2(M_2') + P_0'' A_2'' f_2(M_2'') = P_{0,4} A_4 f_2(M_4) \tag{4}$$

where f_2 is similarly a function of M as given in Eq.5.

$$f_2(M) = \frac{(\gamma M^2 + 1)}{\left(1 + \frac{1}{2}(\gamma - 1)M^2\right)^{\frac{\gamma}{\gamma - 1}}} \tag{5}$$

Then, solving Eq. 4 for M_2'' allows the continuity equation established at section 4 by Eq. 6 to be utilized for calculating the mass flow rate ratios.

$$\mu = \frac{\dot{m}''}{\dot{m}'} = \frac{P_{0,4}}{P_0'} \frac{A_4}{A_1'} \frac{f_3(M_4)}{f_3(M_1')} - 1 \tag{6}$$

f_3 is also a function of the local Mach number ($f_3 = f_3(M)$) as described by Eq.7. Moreover, behaviors of the non-dimensional functions $f_1(M)$, $f_2(M)$ and $f_3(M)$ are provided in Fig.4.

$$f_3(M) = M \left(1 + \frac{1}{2}(\gamma - 1)M^2\right)^{-\frac{\gamma+1}{2(\gamma-1)}} \tag{7}$$

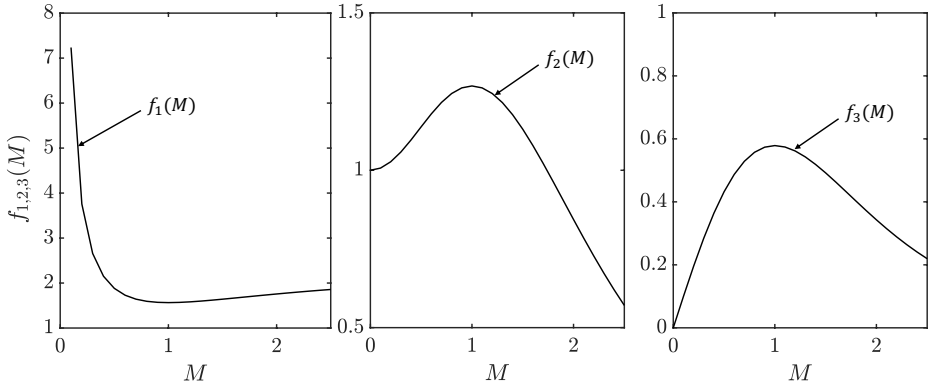

Fig 4. Values of Mach number dependent non-dimensional functions $f_1(M)$, $f_2(M)$ and $f_3(M)$.

2.1.2. Ejector Performance

The ejector performance charts can be investigated in two main regimes referred to as the supersonic and mixed flow patterns where the supersonic regime also contains a saturated flow pattern for sufficiently high secondary stagnation pressure. Since the supersonic flow pattern with sufficient reservoir pressure of the ejector allows the ejector to operate independently from the exhaust pressure, the maximum amount of air flow from the secondary (wind tunnel) stream can be extracted. Accordingly, using Eqs. 1 and 6 the mass flow rate ratios (μ) and the corresponding mass flow rate of wind tunnel stream ($\dot{m}''$) that can be extracted is computed. The results are represented for varying reservoir pressure ratios of secondary and primary streams (P_0''/P_0') at constant wind tunnel stagnation temperature of T_0''=400 K (Fig. 5, left) and varying T_0'' at constant ejector reservoir pressure of P_0'=20 bar (Fig. 5, right). The reservoir pressure of the ejector stream becomes too low to maintain supersonic flow throughout the mixing chamber and mixed flow patterns are observed as indicated by the red shaded area in Fig. 5 (left). Hence, the valid supersonic patterns are obtained to the right side of the dashed region. In terms of mass flow rate ratios (μ), there exists a linearly proportional relationship between μ and P_0''/P_0'. On the other hand, the mass flow rate of wind tunnel stream ($\dot{m}''$) is less dependent on P_0' and dictated mainly by the value of P_0''. Moreover, the temperature dependency of μ and $\dot{m}''$ reveals more dominant effects at higher P_0''/P_0' since with increasing $\dot{m}''$ the contribution of the stagnation temperature of the wind tunnel (T_0'') on the flow properties observed at the mixing chamber is increased. However, as the analysis is performed at constant P_0' (and constant T_0' since there is no temperature control at the ejector reservoir), the mass flow rate of the ejector stream is constant while with varying T_0'' and P_0''. Thus, both $\dot{m}''$ and μ change simultaneously and proportionally.

Furthermore, as the stagnation pressure of the wind tunnel stream (P_0'') is increased, the flow speed of the secondary stream at Section 2 increases to yield chocked flow conditions with M_2''=1 which is referred to as the saturated supersonic regime (Fig. 7). Thus the corresponding μ and $\dot{m}''$ values increase

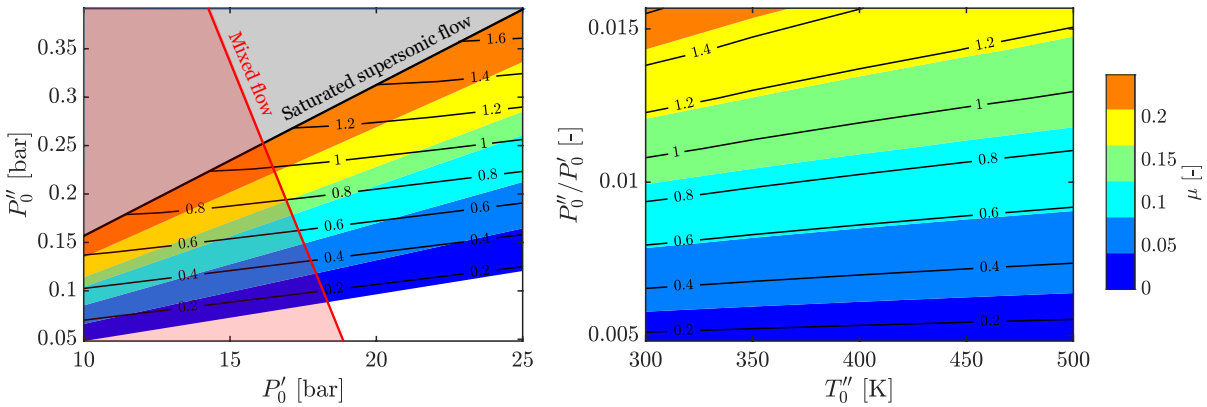

Fig 5. Mass flow rate ratios (μ, colormapped) and mass flow rate (kg/s) of secondary stream ($\dot{m}''$, labeled isolines) with varying stagnation pressures (left) and temperatures for supersonic operation (right). The red and gray shaded areas indicate mixed and saturated supersonic flow patterns respectively (left).

drastically. The trend of linear proportional relationship between μ and P_0''/P_0' becomes more confined to a smaller range due to the small range of P_0'' that can yield a saturated supersonic flow pattern without exceeding the wind tunnel capabilities (Fig. 7, left). Additionally, the dominance of P_0'' on the ejectable mass of air flow from the wind tunnel is observed where it becomes almost independent of P_0'. As the influence of T_0'' analyzed, the aforementioned contribution on flow in the mixing chamber from the secondary stream becomes more profound. Hence the variation of μ and $\dot{m}''$ is affected much predominantly by the wind tunnel stagnation temperature (Fig.7, right). Accordingly, increasing T_0'' at constant P_0'' reduces the density of wind tunnel stream while increasing flow velocity by elevating the local sound of speed. Nevertheless, as the sound of speed is proportional with the square root of local static temperature while the mass flow rate is linear proportional with local density, the resultant mass flow rate of the wind tunnel stream reduces by increasing T_0'' which results in a reduction in μ as well. At suffienctly high P_0'' values where the secondary flow is being chocked at Section 2, the mass flow rate of the wind tunnel stream becomes dominated by the flow properties of secondary flow (P_2'' and T_2'') with little to no influence from primary stream due to the chocking condition which yields the terminology of saturated flow. While for the supersonic flow pattern where the P_0'' lower than the saturation limit, one of the driving factors for the magnitude of $\dot{m}''$ is the formation of the shear layer which acts as the effective compression surface that accelerates the secondary flow stream to meet choking conditions at section 2e (Fig. 3, top). Since the shape of the shear layer is generated by the pressure balance between the primary and secondary streams at section 2, the P_0' value also influences the ejectable mass of air from the wind tunnel test section.

Finally, reducing the ejector reservoir pressure below a limiting value yields a mixed flow pattern where the supersonic flow exiting the ejector nozzle breaks down and becomes subsonic. Hence, throughout the mixing chamber there is a combination of supersonic (at the exit of the ejector nozzle) and subsonic (secondary stream and the downstream ejector stream) flow patterns which puts stringent limitations on the maximum ejectable mass of air from the wind tunnel with an unsteady operational behavior. The mixed flow regime corresponds to a rather confined operational range below which no feasible solution for the wind tunnel operation exists as the ejector experiences unstart [21]. Thus, although the supersonic and saturated supersonic solutions exist below this boundary demonstrated in Fig. 3, these operating conditions are not valid and they are indicated with a red shaded area in Fig. 5 and Fig. 7.

Concentrating on the operational parameters in case of the mixed flow patterns, distinct features can be identified compared to supersonic and saturated supersonic flow patterns. First of all, the trends of mass flow rate of wind tunnel stream ($\dot{m}''$) and ratio of mass flow rates (μ) are drastically different

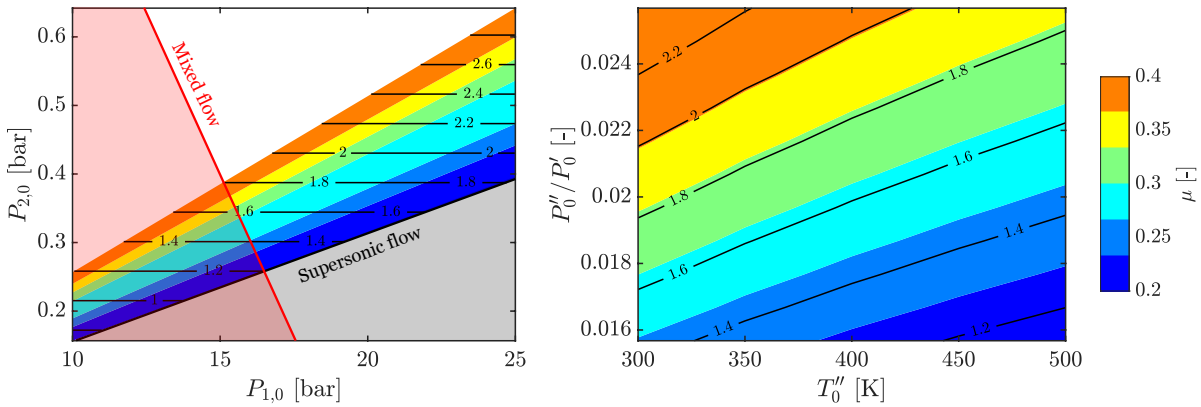

Fig 6. Mass flow rate ratios (μ, colormapped) and mass flow rate (kg/s) of secondary stream ($\dot{m}''$, labeled isolines) with varying stagnation pressures (left) and temperatures for saturated supersonic operation (right). The red and gray shaded areas indicate mixed and supersonic flow patterns respectively (left).

than that of the patterns. Accordingly, changing the ejector reservoir pressure alters the static pressure conditions at section 4. Since the flow exiting the ejector nozzle is still supersonic, varying P_4 values only affect where the shock train of the primary stream breaks and the primary stream transitions to subsonic conditions while not influencing the primary stream properties at the exit of the ejector nozzle (section 2). Thus, the mass flow rate of the primary flow ($\dot{m}'$) and the exiting Mach number (M_2') are still governed by the ejector reservoir pressure and the nozzle geometry. However, due to the fact that the secondary stream is subsonic throughout the mixing chamber, the varying pressure values at section 4 influence the mass flow rate of air ejected from the wind tunnel ($\dot{m}''$). Accordingly, both the mass flow rate ratios (μ) and the mass flow rate of the wind tunnel stream ($\dot{m}''$) becomes considerably dependent on the value of P_0' with a directly proportional relationship where increasing P_0' allows more mass to be ejected from the wind tunnel. This is achieved as increasing P_0' causes the P_4 and M_4 to increase which demands higher momentum at section 2 from the secondary stream at P_0'' to be provided in order to satisfy the momentum balance between section 4 and section 2. Thus, the mass flow rate of the ejector stream and the corresponding mas flow rate ratios increase in a coupled sense.

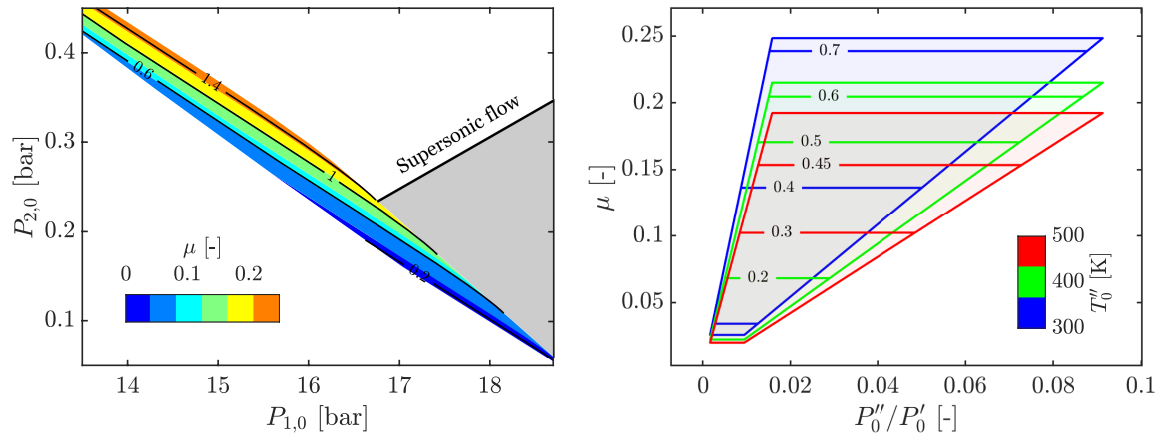

Fig 7. Mass flow rate ratios (μ, colormapped) and mass flow rate (kg/s) of secondary stream ($\dot{m}''$, labeled isolines) with varying stagnation pressures (left) and temperatures for mixed operation (right). The gray shaded areas indicate saturated supersonic flow pattern (left).

Moreover, varying stagnation temperature of the wind tunnel stream alters the mass flow rate of the secondary stream where increasing temperature reduces $\dot{m}''$ due to the inversely proportional quadratic relationship between T_0'' and $\dot{m}''$ (Fig.7). As the operating Mach number of the wind tunnel is aimed to be reduced, the expansion from the stagnation conditions yields higher static temperatures within the test section in comparison to operation at Mach 6. Hence, heating requirements of the dry air supply for preventing condensation are relaxed and the corresponding confinement of the operating regime to lower mass flow rate values will be avoided.

Due to the fact that the desired modifications on the operational range of VKI-H3 wind tunnel require an increase of the mass flow rate through the test section, the strict limitations of the supersonic ejector operation are analyzed to determine the maximum allowable mass flow rate that can be accommodated within the facility. Accordingly, the supersonic flow regime is identified as the most suitable candidate for operating the ejector in order to achieve the desired mass flow rates without overloading the aerodynamic and structural capabilities of the system. Thus, the stagnation pressure of both streams (wind tunnel and ejector) is required to be adjusted accordingly to ensure the operation with supersonic flow patterns throughout the mixing chamber of the exhaust system. Once these conditions can be established, the performed analysis provides the maximum allowable mass flow which can be ejected from the wind tunnel as the supersonic operation regime considering the pressure setting of the ejector stream stagnation conditions shall be adjusted accordingly. Nevertheless, in order for this condition to be ensured, the operating conditions for the mixed regime shall be determined as well to make sure the pressure settings for the ejector reservoir are safely above the transition region. Fig. 5 shows the pressure values of the ejector and wind tunnel stream reservoir relative to the atmospheric exhaust pressure which correspond to the supersonic operating conditions through which the maximum allowable mass flow can be ejected from the wind tunnel $\dot{m}''$=1.8 kg/s which is utilized as the main design constraint in the following sections regarding the nozzle design.

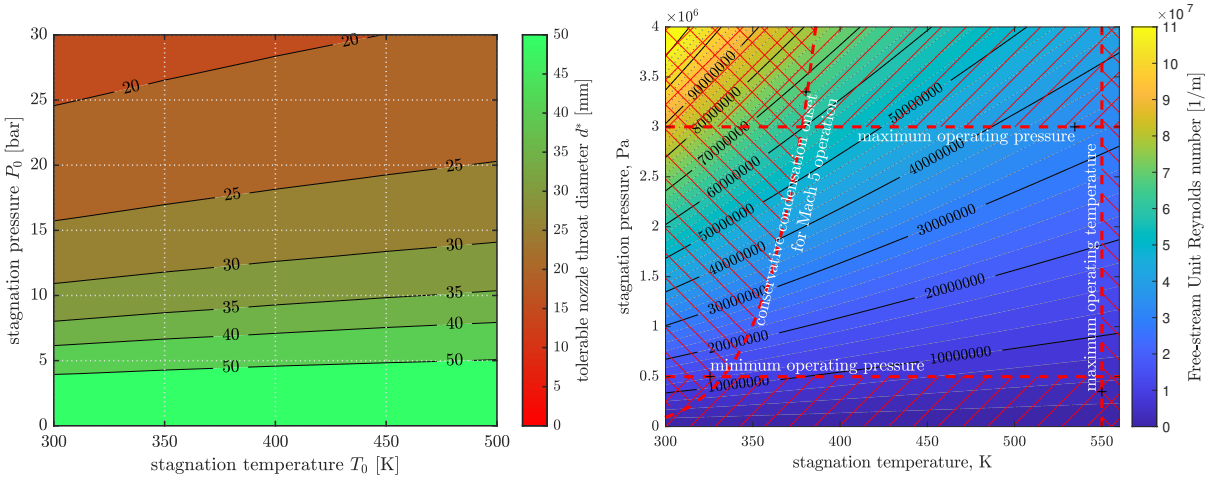

Fig 8. Tolerable nozzle throat diameter d^* (mm) for a given mass flow rate of 1.8kg/s (left). Free-stream unit Reynolds number (right).

2.2. Wind tunnel operational range

The former considerations on the maximum allowable nozzle mass flow rate through the supersonic ejector (1.8kg/s) yield the maximum nozzle throat diameter for any theoretical stagnation pressure and stagnation temperature (Fig. 8, left). On the one hand, the stagnation pressure has a large influence on the tolerable nozzle throat dimensions to achieve a given mass flow rate. The selection of a design stagnation pressure will therefore be governed by the desired nozzle exit diameter. Nevertheless, the stagnation temperature requirements are relaxed with respect to the current tunnel operation at Mach 6 because the flow expansion is less severe and the risk of flow condensation therefore limited. Literature results show that stagnation temperatures on the order of 400K will be enough to conservatively avoid dry air condensation in the test section when expanded to Mach 5. The corresponding operational map

of the tunnel at Mach 5 is depicted in Fig.8 (right). The maximum operating pressure threshold indicated in this figure corresponds to the maximum pressure that can be delivered at the inlet of the nozzle. In practice, lower stagnation pressures will be required to moderate the mass flow rates through the nozzle and ensure compatibility with the supersonic ejector specifications.

3. Design of the new Mach 5 contoured nozzle

3.1. Design methodology

The inviscid nozzle design is first obtained using the method of characteristics implemented within the HYPNOZE code [22] that follows Sivell's methodology [23] . A viscous correction is applied to account for the influence of the boundary layers that develop along the nozzle wall and influence the area ratio of the nozzle. Given the large growth rate of the boundary layer, the nozzle length is cut-off at a location where the inviscid core diameter is the largest [24, 25]. A first evaluation of the viscous effects is achieved based on an empirical correlation [26] and enables parametric studies to be performed (varying design parameters such as the nozzle throat diameter, nozzle throat curvature radius, nozzle maximum opening angle, and nozzle transition length as indicated in Fig. 9). Once a suitable set of design parameters is identified (satisfying the different requirements and dimensional constraints associated with the existing framework of the H3 wind tunnel), an improved viscous correction is obtained through the use of a Navier-stokes flow solver. The numerical results also serve to determine the expected flow uniformity within the test core flow, along both axial and radial directions.

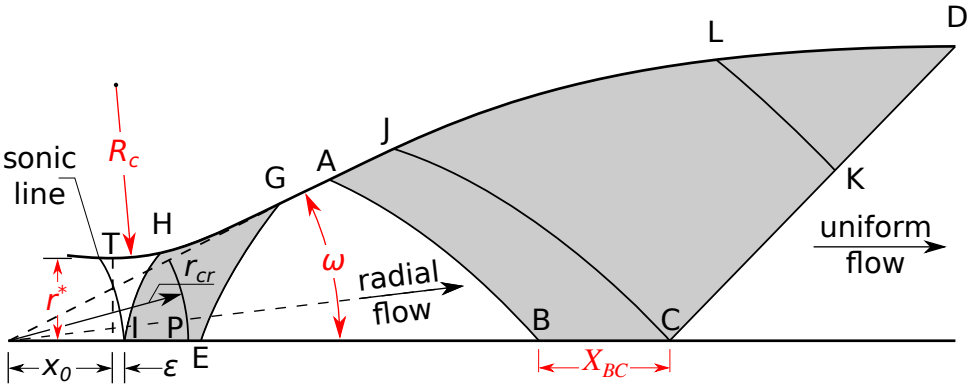

Fig 9. Main design parameters considered in this study.

3.2. Inviscid design

The design parameters of the nozzle throat radius (d^*), the ratio of nozzle throat curvature to nozzle throat radius ($R = R_c/r^*$), the nozzle maximum opening angle (ω) and the nozzle transition length (X_{BC}) are varied within the ranges of $20 < d^* < 30$ mm, $5 < R < 30$ mm, $6 < \omega < 10°$ and $3 < X_{BC} < 6$ mm. Going for a large value of R eases the accurate machining of the throat region (Fig. 10), but also elongates the overall nozzle. Although the influence on the latter is rather weak, the whole inviscid nozzle length increases by 25 mm for the extreme R values considered here. For the following investigations, this parameter R was therefore frozen to $R = 10$ which reduces the design space.

Results of the parametric studies are presented in Fig. 11 as the distance X_{BC} and the opening angle of the nozzle are varied. Emphasis is placed on the analysis of the optimized core diameter, nozzle exit diameter and nozzle length. Results are limited to one throat diameter (namely $d^* = 29mm$) with stagnation flow conditions (namely p_0=1.349MPa and T_0=400K) selected so that the nozzle mass flow rate is compatible with the supersonic ejector specifications. In these figures, blanked areas correspond to sets of design parameters (typically large X_{BC} together with large ω) that did not yield a satisfactory design point. Hatched regions correspond to design parameters that exceed one or several design constraints (minimum/maximum nozzle length, maximum exit diameter, minimum core flow diameter, minimum length X_{BC}). Suitable sets of design parameters are then easily identified. Increasing the transition length X_{BC} elongates the nozzle, reduces the optimized core flow diameter (as a result of the

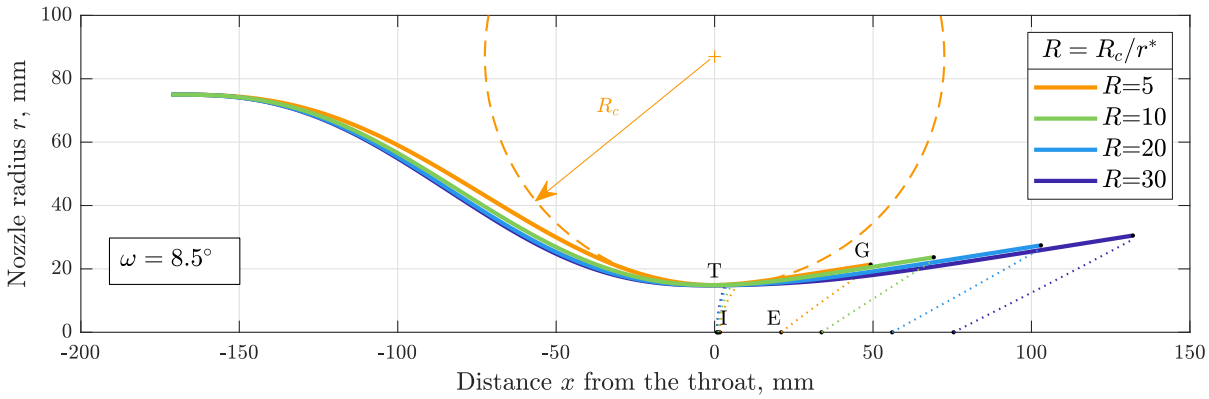

Fig 10. Influence of the nozzle throat curvature radius $R_c = R \times r^*$ on the initial divergent section of the nozzle (downstream contours not plotted).

thicker boundary layers along the contour) and requires slightly larger nozzle exit diameters (again due to thicker boundary layers). Relying on larger nozzle opening angles has the opposite effects, namely requiring shorter nozzles with correspondingly thinner boundary layers which enable larger core flow diameters and smaller nozzle exit diameters. Shallower nozzles are known however to yield better flow quality [27] so this design parameter should be minimized.

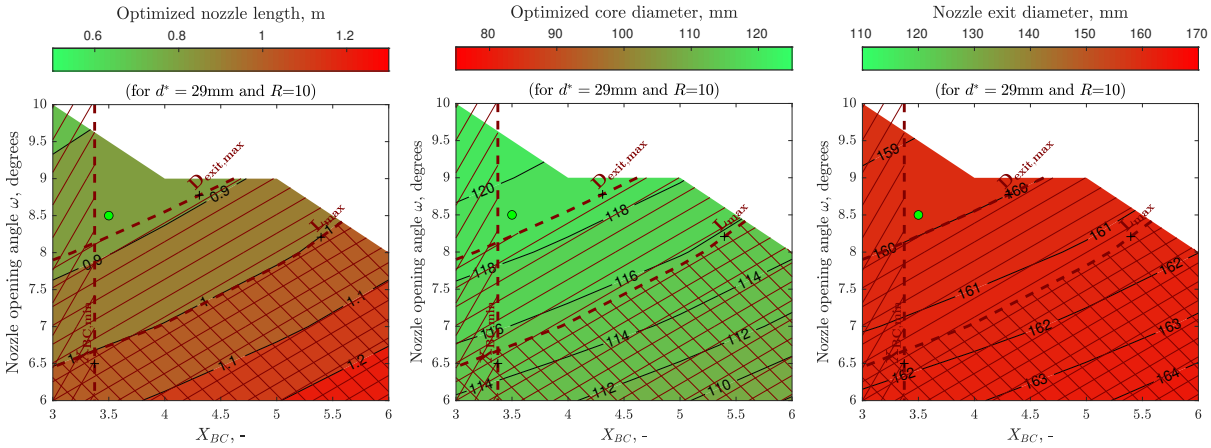

Fig 11. Results of parametric studies (nozzle core flow diameter (left), nozzle core flow diameter (middle) and nozzle exit diameter (right)) showing the variation of nozzle characteristic lengths (after nozzle cut-off) as a function of the transition length X_{BC} and the nozzle opening angle ω. The selected set of design parameters for the new VKI H3 Mach 5 nozzle is indicated with a ● symbol.

Parametric studies show that for a throat diameter of 29mm, a suitable set of design parameters can be found while meeting the different design constraints (minimum/maximum nozzle length, maximum nozzle exit diameter, minimum core flow diameter). One specific set of design parameters corresponding to (P_0=1349 kPa, T_0=400 K, nozzle throat radius=29mm, nozzle throat curvature ratio=10, opening nozzle angle= 8.5°, and transition length=3.5) satisfies the design requirements. The moderate opening angle of the nozzle is expected to benefit the flow uniformity by the nozzle exit. The moderate transition length is favorable for both the nozzle length and the core flow diameter. The latter being conservatively estimated by the empirical correlation, it promises for even larger uniform core flow diameters. A subsonic convergent part is then appended to the nozzle, using a 5th order polynomial, matching first and second derivatives at the inlet and near the throat. The first and second derivatives of the contour are then continuous all along the nozzle, satisfying the usual nozzle design recommendations for improved

flow quality.

3.3. Improved viscous correction

The selected set of design parameters identified in the previous parametric study enables the definition of initial inviscid and viscous contours. Navier-Stokes computations are then performed on the viscous contour in order to improve the accuracy of the viscous correction following an iterative approach. The viscous contour obtained from HYPNOZE is used at first. The corresponding boundary layer displacement thickness is determined along the contour and added to the original inviscid contour issued by HYPNOZE. Another Navier-Stokes computation is then performed on this updated viscous contour. The procedure is repeated until convergence is achieved on the nozzle displacement thickness.

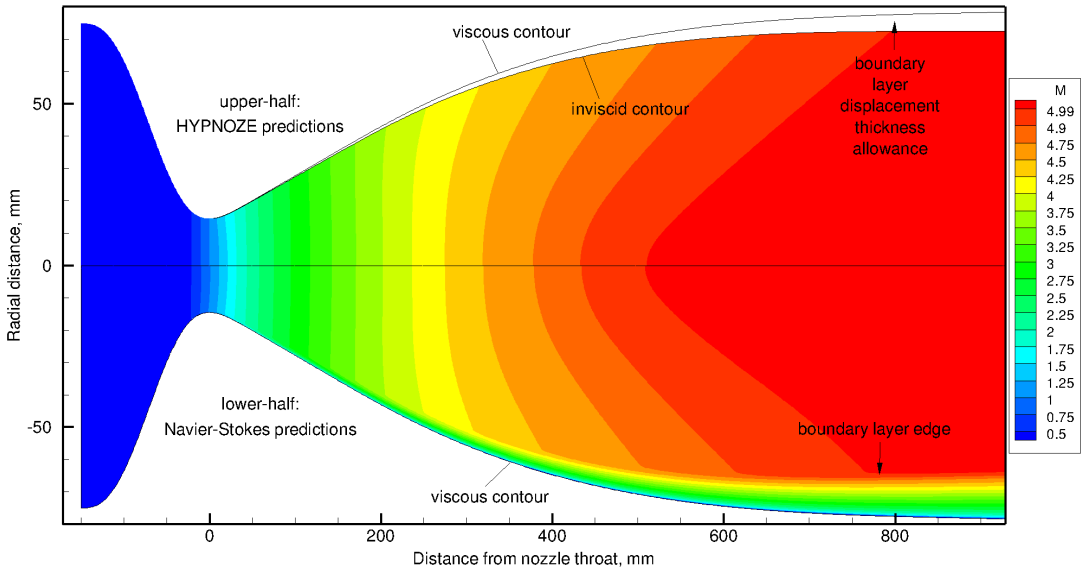

Fig 12. Mach number contours across the nozzle. Upper-half: HYPNOZE predictions. Lower-half: Navier-Stokes predictions.

Stagnation flow conditions at the inlet of the nozzle match the ones used during the HYPNOZE design. Boundary layers are assumed to be fully turbulent where the turbulence is modelled by means of $k-\omega$ turbulence model. The $k-\omega$ SST turbulence model is used. The wall surface temperature is assumed to be isothermal with T_w=300K. This is a realistic assumption in the divergent part of the nozzle owing to the moderate test duration that will be achieved experimentally (closer to the throat, surface temperature changes about 55K may be expected after 10s run duration). Accounting for a more realistic surface temperature distribution is expected to have a negligible influence on the nozzle flow expansion, due to both the moderate expected temperature changes and the relatively thin boundary layers with respect to the inviscid core flow dimensions. Mach number contours within the nozzle and demonstrate the excellent agreement obtained between HYPNOZE predictions and the Navier-Stokes results (Fig. 12). The resulting boundary layer characteristics are shown in Fig. 13.

3.4. Expected nozzle flow uniformity

The Navier-Stokes predictions also serve to estimate the expected nozzle flow uniformity, both along and across the nozzle flow. The flow uniformity along the nozzle centerline (from the theoretical apex of the core flow to the non-optimized full nozzle length) is summarized in Tab. 1. The flow static pressure uniformity is better than 0.8% anywhere along the test rhombus (0.573m$<x<$0.930m) and it further improves approaching the nozzle exit (within 0.1% (95%C.L.) for 0.780m$<x<$0.930m). Similarly, the Mach number scatter along the whole test rhombus is about 0.14% and further improves to 0.02% (95%C.L.) of the targeted Mach number for 0.780m$<x<$0.930m).

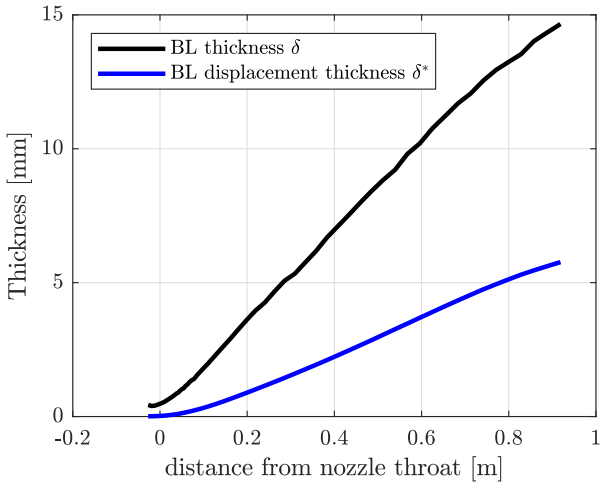

Fig 13. Boundary layer thickness δ (based on 99.5% of the total flow enthalpy) and displacement thickness δ^* along the nozzle contour (for p_0=1.349MPa and T_0=400K).

Detailed comparisons for the flow Mach number and static temperature all along the nozzle centerline are provided in Fig. 14. An excellent agreement is achieved between HYPNOZE and Navier-Stokes. The free-stream static temperature is about 66.8K, which is well above the saturation temperature of the air at the corresponding static pressure. This indicates that the flow will be condensation-free when operated at the selected stagnation flow conditions. The radial flow uniformity is also excellent with variations falling below 0.3% for a 2-sigma confidence level (Tab. 2). The predicted flow angularity is negligible (-0.01°) across the jet. At this location, the inviscid core flow has a diameter of 130mm. Mach number profiles and flow angularity for x =780mm are shown in Fig. **??**, which indicate a very uniform and parallel flow in this plane.

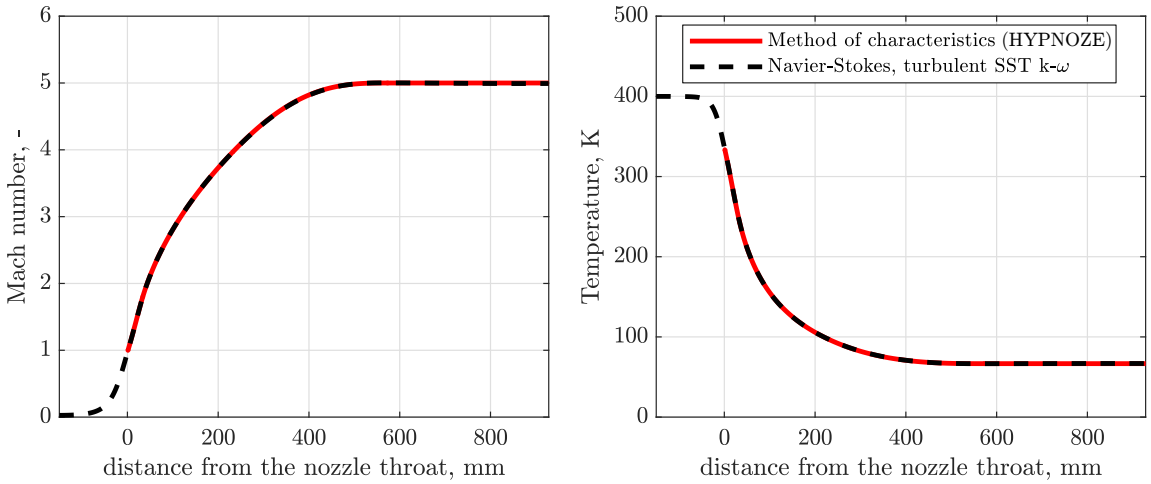

(a) Mach number. **(b)** Static temperature.

Fig 14. Comparison of flow properties along the nozzle centerline as determined by the HYPNOZE design tool and by means of CFD simulations.

The nozzle may be truncated at a length corresponding to the maximum core flow diameter with respect to the boundary layer edge radial location. This occurs at x =780mm from the nozzle throat. Beyond this location, the growth rate of the boundary layer would lead to a reduction of the useful test rhombus. Overall, the selected design for the new Mach 5 contoured nozzle fulfills all technical design criteria and

Table 1. Expected axial flow uniformity (x=0.573 to 0.930m)

Quantity	mean value along test rhombus	1.96σ (95%C.L.)	%
p_∞	2563.4Pa	$\pm$20.6Pa	$\pm$0.80%
T_∞	66.77K	$\pm$0.15K	$\pm$0.23%
ρ_∞	0.134kg/m^3	$\pm$0.001kg/m^3	$\pm$0.57%
u_∞	818.5m/s	$\pm$0.2m/s	$\pm$0.02%
M_∞	5.00	$\pm$0.007	$\pm$0.14%

Table 2. Expected radial flow uniformity in the plane x=780.0mm

Quantity	mean value across inviscid core (for x=780.0mm)	1.96σ (95%C.L.)	%
p_∞	2565.0Pa	$\pm$7.4Pa	$\pm$0.29%
T_∞	66.79K	$\pm$0.20K	$\pm$0.31%
ρ_∞	0.134kg/m^3	$\pm$0.000kg/m^3	$\pm$0.30%
u_∞	818.4m/s	$\pm$0.6m/s	$\pm$0.07%
M_∞	5.00	$\pm$0.011	$\pm$0.22%
θ	-0.01°	$\pm$0.03°	

meets the targeted flow uniformity requirements. The excellent agreement between the HYPNOZE theoretical design and the numerical results also demonstrates that the nozzle flow expansion is free from any disturbance. It is predicted to yield a uniform test rhombus of 130mm diameter by the nozzle exit. The nozzle is currently undergoing the technical design phase and its manufacturing will follow.

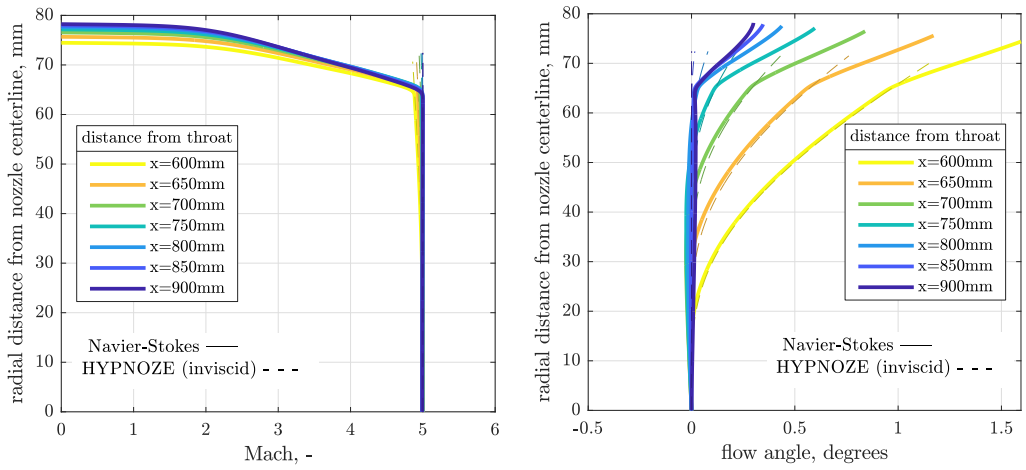

Fig 15. Radial flow Mach number (left) and angularity (right) across the nozzle at x =780mm from the throat.

4. Conclusions

The operational range of VKI H3 hypersonic wind tunnel is extended towards lower speed operation at Mach 5 from Mach 6. This requires a geometric modification of the contoured axisymmetric nozzle for which the capabilities of the other components comprising the operational structure of the wind tunnel are investigated. Accordingly, a major limitation for desired design specifications is observed to be associated with the maximum allowable mass flow rate through the wind tunnel whose extraction from the facility is governed by the performance of the supersonic ejector. Hence, operational range of the available ejector and the maximum mass flow rate that can be accommodated within the wind tunnel is characterized for different operational conditions which provides the final design constraints of the new nozzle. Then, a new contoured axisymmetric Mach 5 nozzle is designed utilizing a method of characteristics based in-house code referred to as HYPNOZE. The provided inviscid contours for the new nozzle are optimized via a parametric study, investigating the entire operational space of the wind tunnel. The optimum design parameters are identified to meet the requirements of the desired modifications enabling operation at high Reynolds numbers. Finally, viscous high fidelity simulations are employed to optimize the boundary layer accommodation through the contours of the nozzle and, to serve as an estimate of the expected quality and uniformity of the core flow.

Acknowledgments

This project has received funding from the European Union's Horizon 2020 research and innovation programme under grant agreement No 101006856.

References

[1] W. Dieudonne, H.L. Boerrigter, and J.M. Charbonnier. Hypersonic flow on a blunted cone-flare and in the vki-h3 mach 6 wind tunnel. 1997.

[2] R. Savino and D. Paterna. Blunted cone–flare in hypersonic flow. *Computers & Fluids*, 34(7):859–875, 2005.

[3] R. Donelli, A. Schettino, J. Perraud, D. Fletcher, and S. Paris. *Design of a Laminar-Turbulent Transition Flight Experiment*. 2005.

[4] S. C. Tirtey, O. Chazot, and L. Walpot. Characterization of hypersonic roughness-induced boundary-layer transition. *Experiments in Fluids*, 50(2):407–418, Feb 2011.

[5] G. Grossir, D. Masutti, and O. Chazot. *Flow characterization and boundary layer transition studies in VKI hypersonic facilities (Invited)*. 2015.

[6] D. Masutti, O. Chazot, R. Donelli, and D. de Rosa. Design and Ground Testing for the EXPERT PL4/PL5 Natural and Roughness Induced Transition. Noordwijk, 2011. ESA Communications.

[7] D. Masutti, E. Gunaydinoglu, and O. Chazot. Surface Pressure Measurements On A Flat Plate And A 7DEG Half-Cone At Mach 6. In L. Ouwehand, editor, *7th European Symposium on Aerothermodynamics*, volume 692 of *ESA Special Publication*, page 78, May 2011.

[8] A. Turchi, S. Paris, W. Agostinelli, F. Grigat, S. Löhle, D. Bianchi, and L. Ferracina. Assessment of the effect of heat-shield ablation on the aerodynamic performance of re-entry capsules in hypersonic flows. 07 2019.

[9] D. Masutti, S. Bernhardt, C. Asma, and M.R. Vetrano. *Experimental Characterization of Liquid Jet Atomization in Mach 6 Crossflow*. 2009.

[10] C. O. Asma, S. Tirtey, and F. Schloegel. Flow topology around gas, liquid and three-dimensional obstacles in hypersonic flow. *AIAA Journal*, 50(1):100–108, 2012.

[11] G. Simeonides. The VKI hypersonic wind tunnels and associated measurement techniques. Technical Memorandum VKI TM-46, von Karman Institute for Fluid Dynamics, November 1990.

[12] D. Masutti, E. Spinosa, O. Chazot, and M. Carbonaro. Disturbance level characterization of a hypersonic blowdown facility. *AIAA Journal*, 50(12):2720–2730, 2012.

[13] P. W. Agostinelli, A. Turchi, D. Le Quang, D. Masutti, L. Vigevano, D. D'Ambrosio, and O. Chazot. *Investigation of Hypersonic Flow in the VKI H3 Wind Tunnel: from Facility Characterization to Boundary-Layer Interaction over Low-Temperature Ablators*. 2020.

[14] W. Kordulla. *Calibration of the hypersonic blow down wind tunnel H-3*. 1970.

[15] J. L. Vanhee. *The H-3 hypersonic wind tunnel: new implementation and calibration,*. 1989.

[16] J. Fabri and R. Siestrunck. Supersonic air ejectors. volume 5 of *Advances in Applied Mechanics*, pages 1–34. Elsevier, 1958.

[17] J. C. Dutton and B. F. Carroll. Optimal Supersonic Ejector Designs. *Journal of Fluids Engineering*, 108(4):414–420, 12 1986.

[18] A. Hemidi, F. Henry, S. Leclaire, J.-M. Seynhaeve, and Y. Bartosiewicz. Cfd analysis of a supersonic air ejector. part ii: Relation between global operation and local flow features. *Applied Thermal Engineering*, 29(14):2990–2998, 2009.

[19] R. S. Benson and V. A. Eustace. A study of two-dimensional supersonic air ejector systems. *Proceedings of the Institution of Mechanical Engineers*, 187(1):733–743, 1973.

[20] M. V. Srisha Rao and G. Jagadeesh. Mixing in a supersonic ejector - an experimental investigation. In R. Bonazza and D. Ranjan, editors, *29th International Symposium on Shock Waves 2*, pages 907–912, Cham, 2015. Springer International Publishing.

[21] V. Lijo, H. Dong Kim, S. Matsuo, and T. Setoguchi. A study of the supersonic ejector–diffuser system with an inlet orifice. *Aerospace Science and Technology*, 23(1):321–329, 2012. 35th ERF: Progress in Rotorcraft Research.

[22] G. Grossir and O. Chazot. *Design of axisymmetric contoured nozzles for calorically and thermally imperfect gases using the HYPNOZE code*. 2022.

[23] J. C. Sivells. A computer program for the aerodynamic design of axisymmetric and planar nozzles for supersonic and hypersonic wind tunnels. Technical Report AEDC-TR-78-63, Arnold Engineering Development Center, December 1978.

[24] Y.-N. Yu. A summary of design techniques for axisymmetric hypersonic wind tunnels. In *AGARDograph35*. NATO, November 1958.

[25] J. Lukasiewicz. *Experimental methods of hypersonics*. Marcel Dekker, Inc, 1973.

[26] E. Edenfield. *Contoured nozzle design and evaluation for hotshot wind tunnels*. 1968.

[27] F. L. Shope. Contour design techniques for super/hypersonic wind tunnel nozzles. In *24th AIAA Applied Aerodynamic Conference*, number AIAA paper 2006-3665, June 2006.